18

Microwave Properties of Dielectric Materials

JS Mandeep[1] and Loke Ngai Kin[2]
[1]Department of Electrical, Electronic & Systems Engineering
[1]Institute of Space Science,
Faculty of Engineering & Built Environment
Universiti Kebangsaan Malaysia
43600 UKM Bangi
Selangor Darul Ehsan,
[2]School of Electrical and Electronic Engineering,
Universiti Sains Malaysia, Nibong Tebal,
Engineering Campus 14300, Pulau Pinang,
Malaysia

1. Introduction

In recent years, the study of newer types of dielectric materials and compositions has been of great interest. The quest for new, innovative and easily obtainable dielectric materials that yield predictable and controllable permittivity and permeability values with very low dielectric loss has always been fruitful. New ideas and designs to implement these materials in microwave devices and structures with the most efficiency and performance are also of equal importance.

The book chapter covers the synthesis and characterization of new dielectric material compositions and the design, implementation and testing of a prototype dielectric resonator antenna and filter utilizing the fabricated dielectric material. It also covers the use of different design and testing techniques in this research. By studying different methodologies and new material types that were previously published in cited technical journals such as Science Direct, different types of materials and synthesis methods were able to be identified. The appropriate materials and method of synthesis were then derived and utilized in the fabrication of the new type of dielectric ceramic substrate material.

After extensive literature reviews, research and analysis, various methods used in dielectric resonator designs were studied and analyzed. An overview of the synthesis process associated with the fabrication of the new dielectric composition will be discussed. Next, with the primary objective of investigating the microwave properties of a new composition of high permittivity ceramic dielectric substrate at microwave frequencies, research is then carried out on designing an electrical model in order to utilize the newly fabricated dielectric material in a microwave environment. The electrical model that is proposed will be of dielectric resonator devices which will incorporate the new dielectric material type. Tests and measurements will also be carried out at various microwave frequencies in order

to study the behaviour of the dielectric material. Different shapes and thicknesses of the dielectric material will also be studied to observe the effects they have towards the characteristics of the electrical model at microwave frequencies. Lastly, analysis will be carried out for these variations in order to determine the characteristics and the traits of the dielectric designs at microwave frequencies.

2. Microwave properties of dielectric materials

2.1 Barium strontium titanate

Two batches of pre-synthesized Barium Strontium Titanate (BST) pellets were provided by the School of Material Engineering for dielectric characterization and testing at microwave frequencies. They will also provide a starting template as a dielectric model in CST in order to design the dielectric resonator antenna and filter that will be used with the Bismuth Lanthanum Titanate pellets. These BST samples will provide an overview on the dielectric characteristics and properties of similar ceramic substrates. Thus, it will be easier to transfer the BST dielectric initial designs to accommodate uncharacterized BLT materials that were not ready during the electrical model design process. The most important reason for the analysis of these pre-made samples is to study the effects of different variations in the synthesis process towards the performance and dielectric properties of the material.

For Barium Strontium Titanate, there are two batches of samples which are Type A and Type B. Type A being the batch of samples synthesized via mixed oxide heat treatment method and Type B is the batch that was prepared using wet chemical method. While it is observed that the value of permittivity varies in relation with the measurement frequency (especially in the high frequency range), all measurements were carried out at 1.4GHz as it best represents the dielectric properties in the range of operating frequency where it is used in the electrical model.

2.2 Type A (mixed oxide heat treatment) 1.4GHz

By using the HP 4291B Material Analyzer connected to the permittivity test head, the dielectric properties of the samples are measured at the sweep frequency of 1.4GHz. It is also noted that the maximum measurement frequency for the analyzer is limited to 1.8GHz, thus the dielectric properties of the test material at frequencies higher than 1.8GHz could not be measured. The samples were first cleaned and polished at the contact planes for maximum contact with the test probes with minimal air gaps. The measured dielectric properties are presented in the following table and figures.

Type A	Permittivity, ε_r	Loss Tangent	Thickness (mm)
1	110.74	5.58E-02	2.85
2	299.62	2.25E-01	2.74
3	-120.34	5.98E-01	2.30
4	64.364	1.3568	2.48

Table 1. Dielectric Properties of Type A Samples.

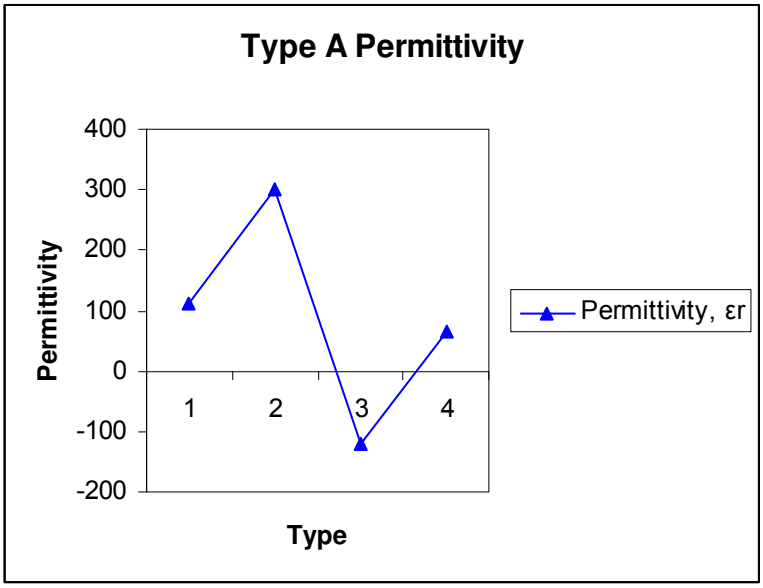

Fig. 1. Type A Permittivity Trend.

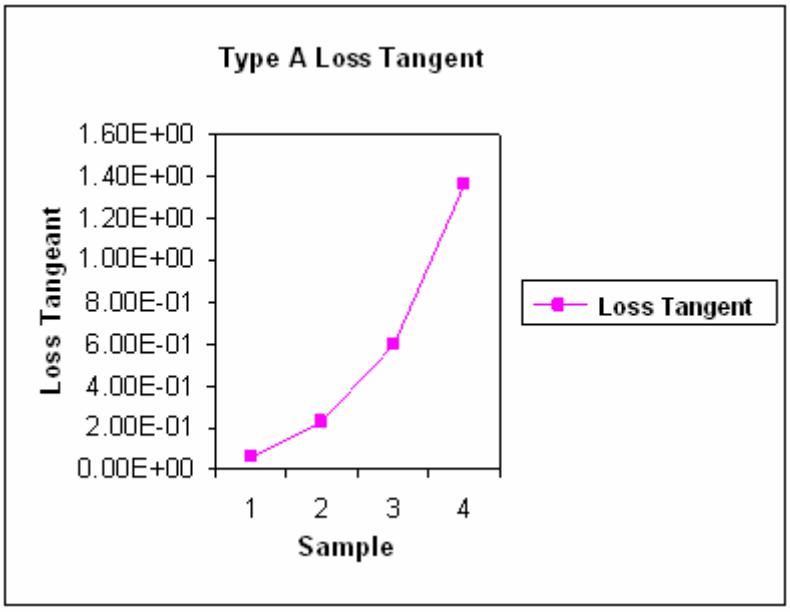

Fig. 2. Type A Loss Tangent Trend.

Observing the permittivity characteristics obtained from the Material Analyzer, the Type A samples has an ideal maximum permittivity condition at Sample 2. The Samples 1, 2, 3 and 4 are each synthesized at 1100˚C, 1200˚C, 1300˚C and 1400˚C respectively. Interestingly, Sample 3 is observed to be measured with a real negative vector value of permittivity. A dielectric material measured having these negative ε or μ values indicates that electric fields (ε) or magnetic fields (μ) entering the material has a negative refraction angle, meaning the field lines do not penetrate the material, but reflecting off it and is opaque to electromagnetic radiation. Rare types of materials with both negative values of permittivity and permeability are known as metamaterials where the dielectric properties are now affected by the structural properties of the material itself and not the composition of molecules. [19-21] As the permeability of the sample in test cannot be measured at the moment using the existing analyzer without the permeability test head, it is uncertain if Sample 3 is of metamaterial characteristics. However it is known that Sample 3 exhibits a negative real part of permittivity thus meaning that the refraction angles of penetrating electromagnetic field lines are negative as well rendering the material opaque to electric fields. The study of this material however, will not be covered in this project as further studies are still needed in this relatively new topic of research.

2.3 Type B (wet chemical method) 1.4GHz

Dielectric measurements were taken for the Type B batch of samples that were synthesized using wet chemical method on the same measurement setup. Similarly, the samples were cleaned and polished at the contact planes for maximum contact with the test probes with minimal air gaps. Variations of dopant ratios were introduced into the individual samples in order to observe the effect on the dielectric properties at microwave frequencies. It is noted that the thickness of each sample is kept constant at 1.15mm for this batch. However, it is understood that the thickness of the samples will not have any effect on the measurement results. The measured dielectric properties are presented in the following table and figures.

Type B	Strontium Dopant % Ratio	Permittivity, ε_r	Loss Tangent	Thickness (mm)
1	1	103.34	1.52E-01	1.15
2	0.9	43.95	7.91E-02	1.15
3	0.7	118.23	8.35E-02	1.15
4	0	60.658	2.46E-03	1.15

Table 2. Dielectric Properties of Type B Samples.

Dielectric properties for Type B samples which are synthesized via wet chemical method shows normal distribution of permittivity and loss relative to the composition ratio of Strontium dopants in the samples. It is noted that the maximum permittivity is obtained from the percentage ratio of 0.7 and the maximum loss, meanwhile is obtained from the ratio of 1. This indicates that the introduction of Strontium dopants in the dielectric material increases the loss tangent of the electric fields passing through the sample. The excess Strontium atoms doped in the crystalline lattice might have introduced dampening to the electromagnetic waves that were propagating through the material. By using wet chemical method in synthesizing the samples, no negative permittivity or permeability properties

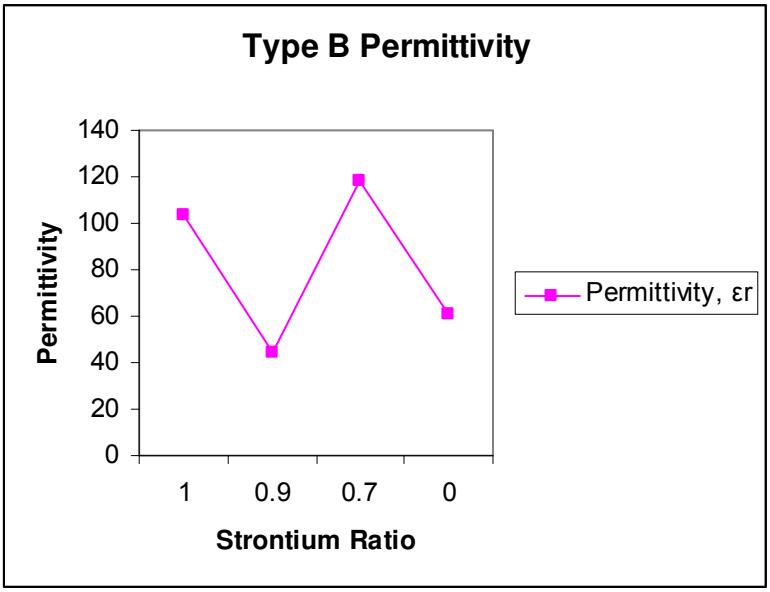

Fig. 3. Type B Permittivity Trend.

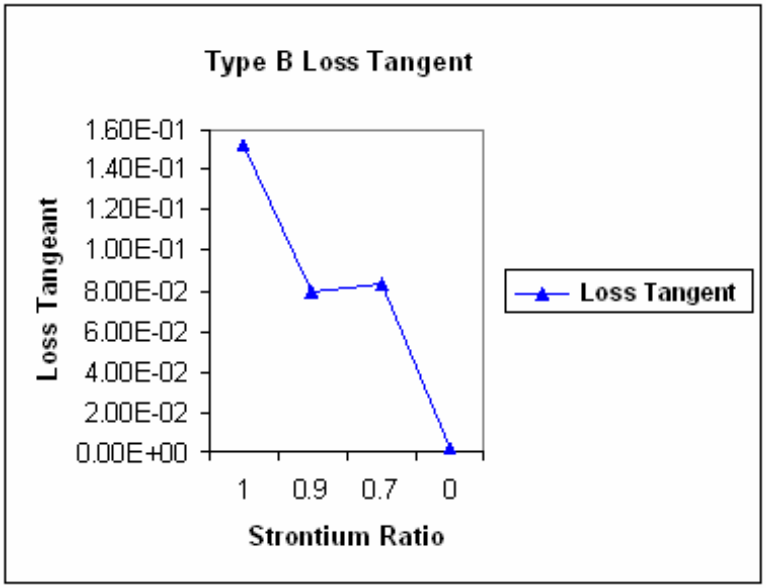

Fig. 4. Type B Loss Tangent Trend.

were observed among the samples. This also suggests that by using the wet chemical method, no significant structural atomic properties were formed during synthesis as opposed by the heat oxide treatment method.
Unlike the mixed oxide synthesis method which requires considerable amount of heat to form crystalline molecular bonds inside the material, no significant atomic alteration occurred for these samples thus retaining more typical properties. From the observation of the samples in comparison with the previous Type A samples, it is obvious that wet chemical method is more suitable as a synthesis process for high permittivity, doped, ceramic dielectric materials. It is also observed that keeping the dopant ratio below 0.7 yields the best dielectric characteristics for the material. From the results and analysis of the dielectric properties displayed by BST synthesized via different techniques, the best method and process was able to be roughly determined for the synthesis of Bismuth Lanthanum Titanate.

2.4 CST simulation and measurement results and comparison
2.4.1 DRA results
The design that was constructed in CST was exported into DXF format to be photo-etched onto a Rogers type double-sided copper-clad substrate. The substrate measured with permittivity of 3.5398, loss of 4.5364E-03 and thickness of 0.80mm. A 50Ω SMA connector is used at the feed of the strip line. Meanwhile for consistency, the sintered and polished pellets are then measured again using a HP Material Analyzer for their permittivity and dielectric loss values at 1.4GHz. The sample with 0.5 doping ratio was selected for the ideal test sample as it has the best solid form and also good dielectric properties. The sample is very dense and is not brittle or porous compared to the other samples which are less desirable. Its measured permittivity and loss are ε_r = 94.243 and tanδ = 6.654E-03 respectively. The dielectric samples will be shaped into the various shapes previously discussed for measurements and comparison in the following sections. Plate 4.3 shows the fabricated DRA on a Rogers double sided substrate board.

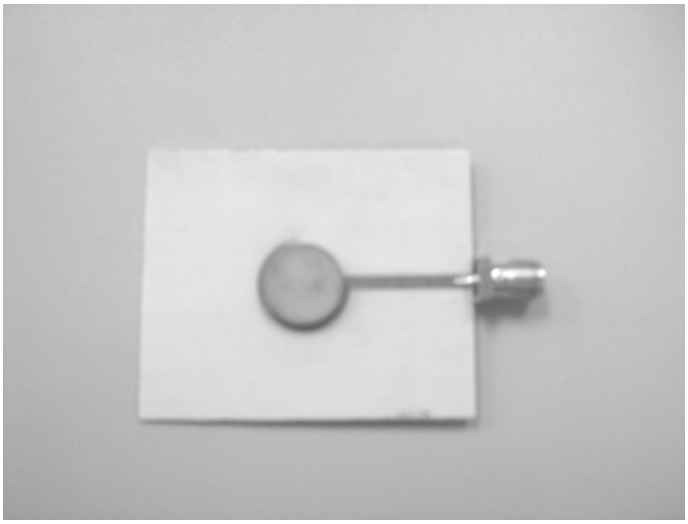

Fig. 5. Dielectric Resonator Structure.

2.4.2 Cylindrical pellet

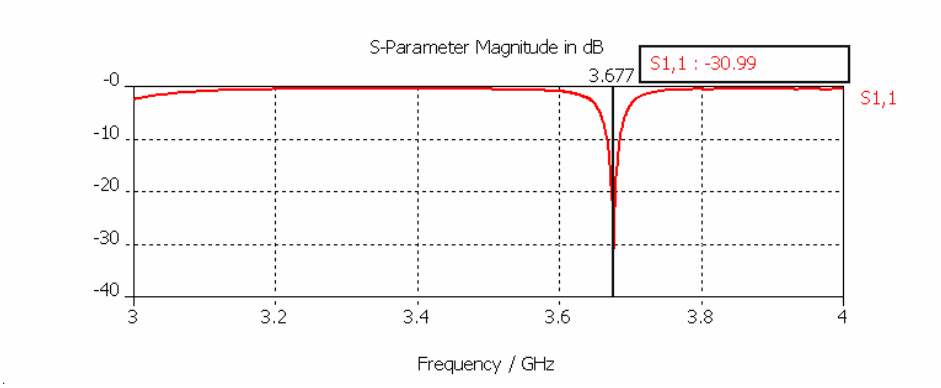

Fig. 4.5. S(1,1) Frequency Response of DRA Structure.

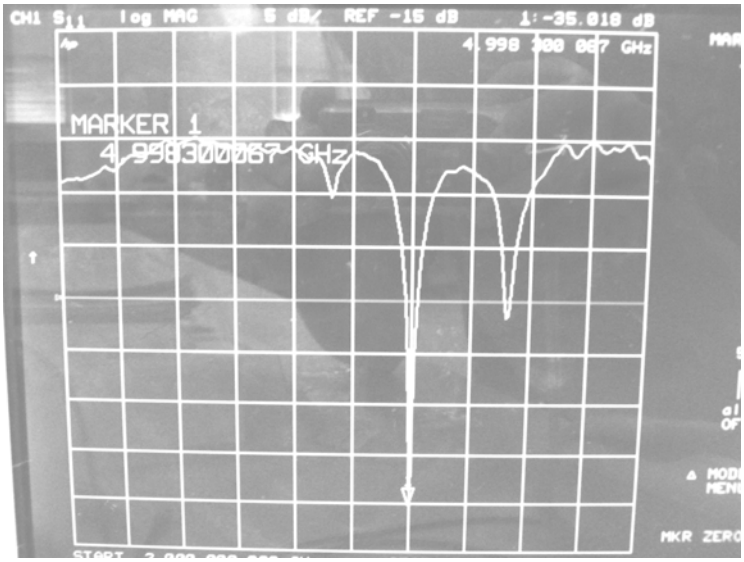

Fig. 6. Measured S(1,1) Frequency Response of DRA Structure.

Figure 6 shows the simulated and measured S(1,1) frequency response of the resonator structure at a sweep frequency range of 3GHz to 4GHz. The resonant frequency is iteratively tuned to 3.677 GHz. By varying the strip length and width, the resonant frequency can be shifted accordingly. Comparison with the simulated response showed a 35% frequency shift at 4.998GHz on the actual measured response at -35.010dB. This is expected as there is some slight known tolerance in the fabrication of the PCB and also of the non constant microwave characteristics of the dielectric material at different microwave frequencies. Input impedance at the input port is at 52.4 – 1.605j Ω at resonance frequency of 3.677 GHz which is close to the desired 50Ω. Simulated and measured impedance response for the frequency range is shown below in Figure 7 and Figure 8 respectively.

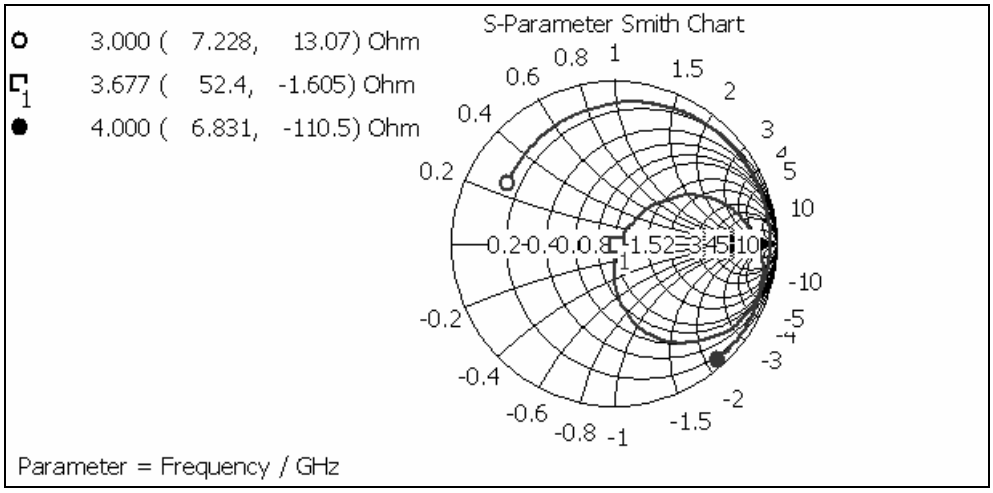

Fig. 7. Input Impedance Response of DRA Structure.

Fig. 8. Measured Input Impedance of DRA Structure.

Figure 9 shows the simulated radiation pattern and characteristics for the resonator operating at its simulated resonant frequency at 3.677GHz. The radiation pattern is a ϕ-Plot in which the radiation is observed at a parallel plane with the DRA. As observed, the attenuation characteristic of this DRA towards the radiation reduces radiation efficiency and transmission power. Thus, it is noted that this DRA design has a tendency to suppress or attenuate electromagnetic radiation. It is in essence, not an efficient electromagnetic radiator structure. However, it is greatly preferred in pure resonator or RF load applications where electromagnetic radiation is undesirable. The actual radiation pattern is not measured due to

its poor radiation properties. However, from this simulation we know that this particular type of dielectric resonator design can be modified into an efficient microwave filter structure that does not require electromagnetic radiation. Further explanation on this is as follows.

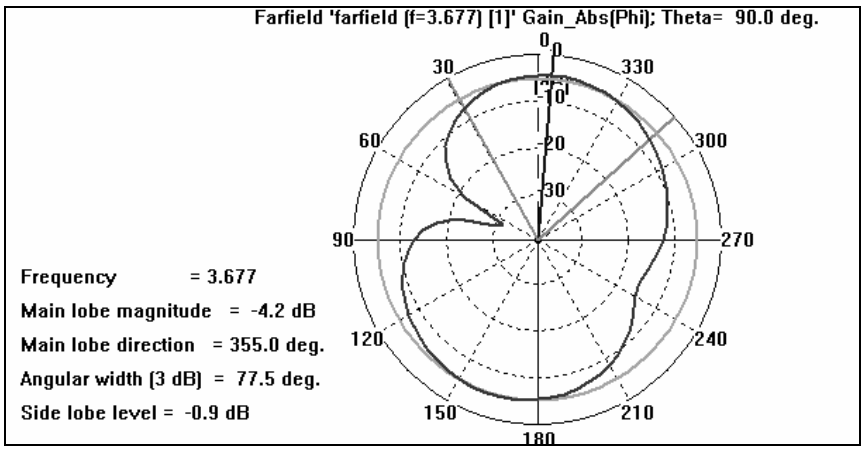

Fig. 9. Radiation Pattern and Properties of DRA Structure (ϕ-Plot).

Most dielectric resonator antennas or array antennas radiate from a single sided plane, in which fields fringing from the conductor edges towards the ground plane transmit radiation energy. The gain or directivity in dBi can be altered so that the radiation energy is focused into a specific direction or pattern, as shown in radiation pattern plots. The value of 0dBi refers to the absolute gain value of 1, which is the gain produced by an isotropic antenna in which radiation power is uniformly distributed at all angles. However, values of dBi which are negative in this case mean that the DRA is attenuating the radiation energy making it less efficient as a radiating device. In this case, it is an ideal configuration for a non-radiating resonator device. Dielectric resonator designs like this can sometimes be derived into filters, couplers and mixers that do not require energy radiation into free space. Thus, the need for extensive RF shielding can be minimized for this type of device. This means that costly metallic shielding enclosures are no longer needed to ground the electromagnetic fields that radiates from the resonator structure.

From further analysis, the high permittivity dielectric material placed in the center of the microstrip ring alters the natural input impedance of the microstrip patch and matches it to 50Ω at its resonant frequency. This enables the mismatched microstrip patch to resonate at its natural resonant frequency. The design of a dielectric resonator filter was also able to be derived from this basic dielectric resonator antenna structure as the excitation mode that is generated by the microstrip ring coupling creates confined $TM_{01\delta}$ radiation. This design will be tested and measured in the later DRF section. The use of various dielectric shapes and variations is observed in the following sections below.

The measurement tests carried out on the dielectric resonator filter device is similar to the DRA with the exception of the filter being a two port device. Thus, the S-parameters will be the measured for S(1,2) and S(2,1) in order to obtain the frequency response of the filter at the operating frequency range of 1-3GHz. The HP Network Analyzer shown in Figure 10 is

used to measure the S-parameters and also the impedance of the filter device at the determined frequency range. Additionally, a power transmission measurement will be carried out on the filter device to further observe the actual application and response of the filter in a proper transmission circuit. The circuit diagram and also the actual test configuration for this measurement setup are illustrated and shown in Figure 11 and Figure 12 on the following page.

The design that was constructed in CST was exported into DXF format to be photo-etched onto a Rogers type double-sided copper-clad substrate. The substrate measured with permittivity of 3.5398, loss of 4.5364E-03 and thickness of 0.763mm. A 50Ω SMA connector is used at the feed of the microstrip transmission line at both ports. Meanwhile, the sintered and polished pellets are then measured again using a HP Material Analyzer for their permittivity and dielectric loss values at 1.4GHz for consistency. The sample pellet piece

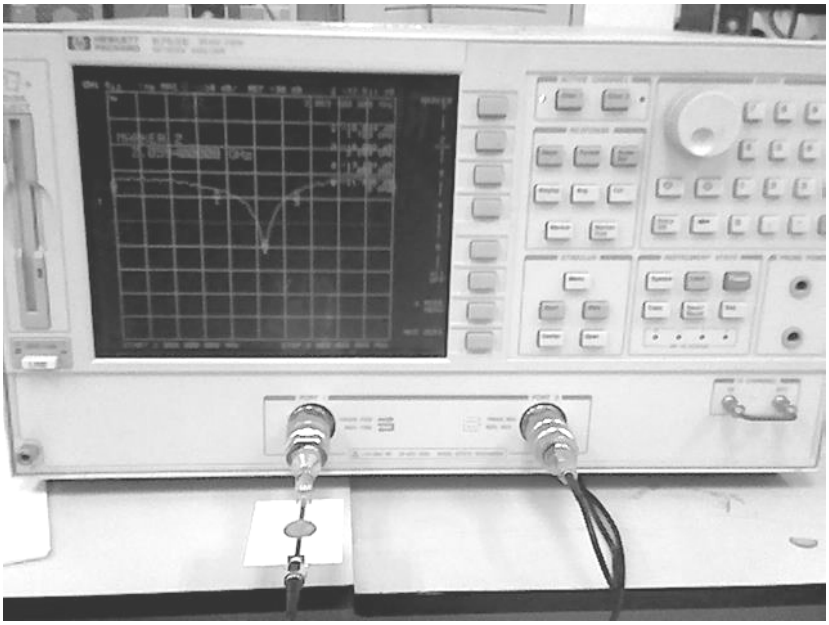

Fig. 10. DRF S(1,2) Measurement Setup.

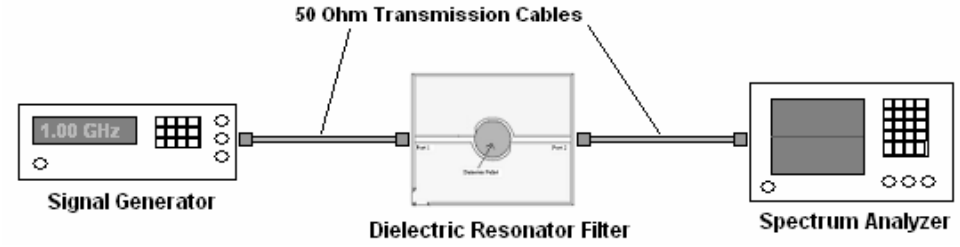

Fig. 11. DRF Power Transmission Measurement Setup Diagram.

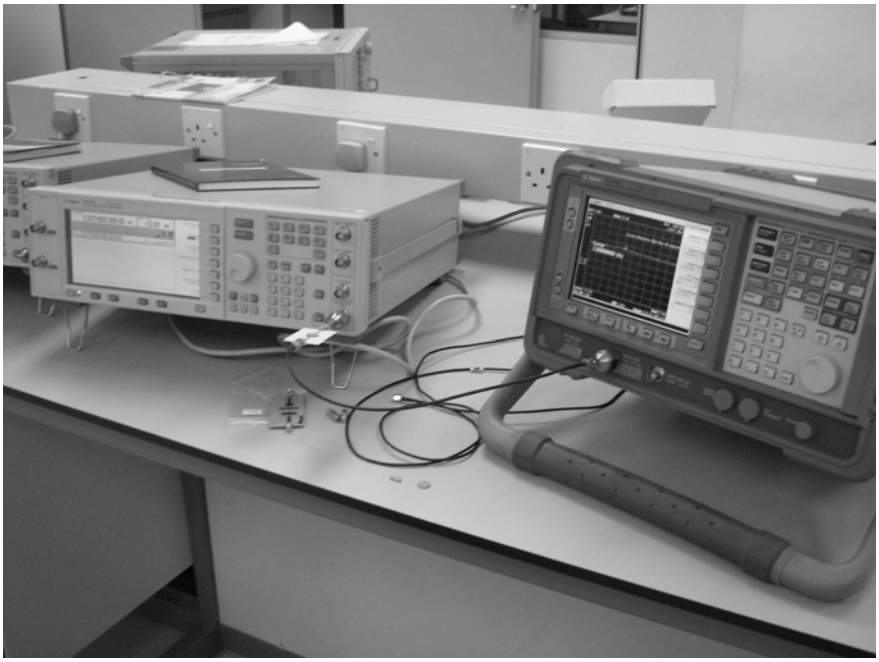

Fig. 12. DRF Power Transmission Measurement Setup.

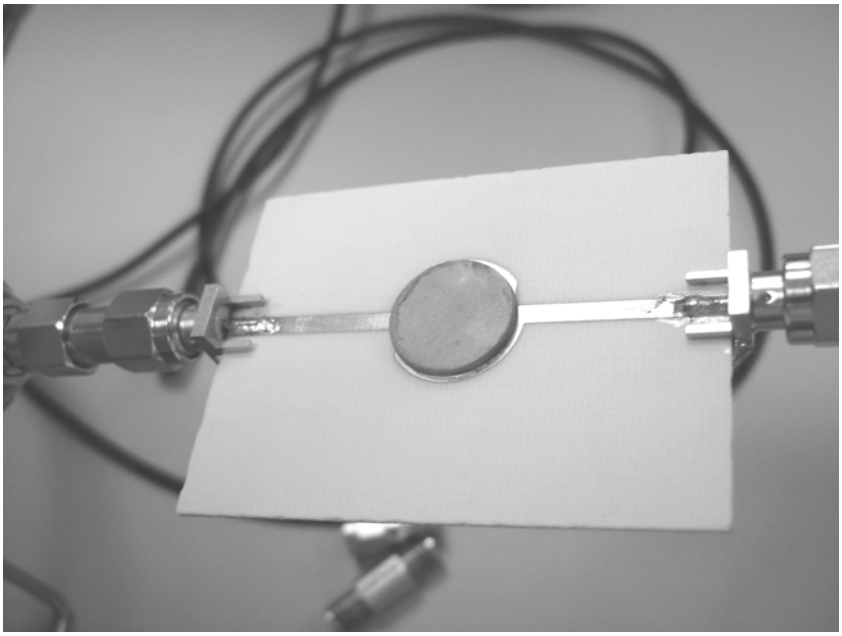

Fig. 13. Dielectric Resonator Filter Structure.

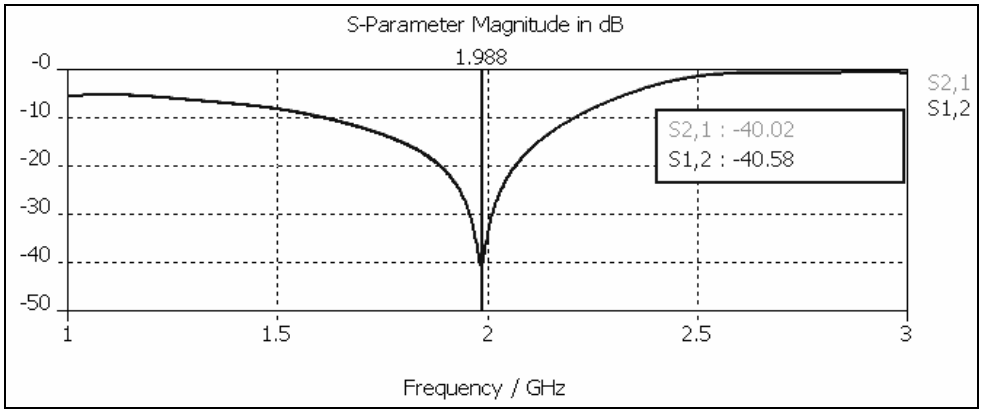

Fig. 14. S(1,2) and S(2,1) Frequency Response of DRF Structure.

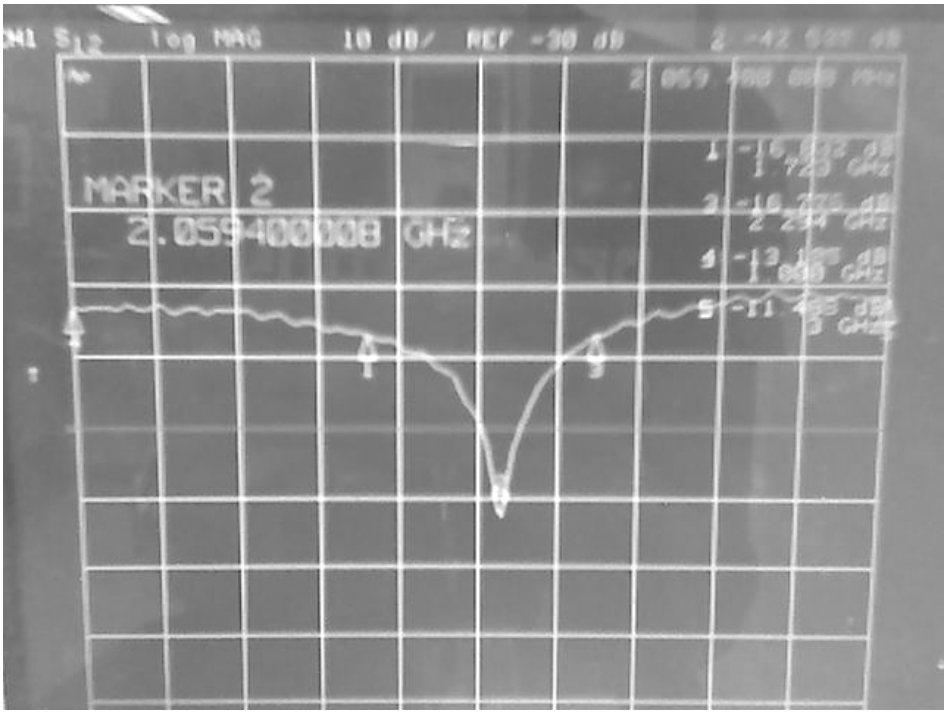

Fig. 15. S(1,2) Measured Frequency Response of DRF Structure.

with 0.5 doping ratio that was sintered at 1000˚C was observed and measured to have a good solid form and also good and consistent dielectric properties. The sample is very dense and is not brittle or porous. Its measured permittivity and loss are εr = 49.416 and tanδ = 20.296E-03 respectively. The thickness of the sample is measured at 1.15mm. It is selected for use with the filter structure.

Figure 14 above shows the simulated S(1,2) and S(2,1) frequency response of the resonator structure at a sweep frequency range of 1GHz to 3GHz. The DRF structure exhibits a bandstop type filter response. The bandstop center frequency was fine tuned to 1.988 GHz by varying the strip lengths and width during the iterative tuning process in CST. The filter is connected to the HP Network Analyzer to measure its S(1,2) and S(2,1) response at a test frequency range 1.5GHz to 2.5GHz. The test setup used was shown in Figure 12. As the dielectric resonator filter in test is symmetrical, thus only the S(1,2) response data is collected since it will be the same for S(2,1). The actual S-parameter measurement obtained from the network analyzer is shown in Figure 14. The actual measurements are verified to be the same as the simulated response and by comparison, the actual measurements show a better symmetry at both the low and high bandpass frequency spectrum of the filter. The notch filter center frequency is measured at 2.059GHz at -42.579dB. The key measurement points and -3dB levels at 1.723GHz and 2.294GHz for the S(1,2) response curve of the filter are listed in Table 3.

Frequency (GHz)	S(1,2) (dB)
1.000	-13.208
1.723 (-3dB)	-16.839
2.059	-42.579
2.294 (-3dB)	-16.786
3.000	-11.495

Table 3. S(1,2) Measurement Values

Based on the measurement values obtained from the network analyzer, the bandwidth and also the quality factor (Q-factor) for the DRF can be calculated. The bandwidth for all microwave filters is obtained from the frequency range of the -3dB gain cutoff levels derived from their respective S(1,2) or S(2,1) plots shown in Table 4.4. The bandwidth of a filter represents the range of frequencies in which the device passes or stops, depending on the type of filter being used. The Q-factor however defines the quality of frequency separation for microwave filter in question. For example, a microwave bandpass filter with a high Q-factor enables the cutoff frequencies to be more precise and distinct, which in graphical terms mean a steeper cutoff frequency slope. As an example, a Butterworth filter has the lowest Q-factor of all other known filter types because of its more gradient cutoff. For this notch filter DRF, the bandwidth is calculated at 571MHz while the Q-factor is at a very acceptable value of 3.6. The calculation for the bandwidth and Q-factor of the DRF are shown in the following expressions.

$$Bandwidth\,(MHz) = 2.294\,GHz - 1.723\,GHz = \underline{\underline{571\,MHz}} \tag{1-a}$$

$$Q\text{-}Factor = \frac{Center\ Frequency}{Bandwidth} = \frac{2.059\,GHz}{0.571\,GHz} \tag{1-b}$$

$$= \underline{\underline{3.6}}$$

In order to measure the power transmission for the filter, the filter is connected to a signal generator and spectrum analyzer as shown previously. Figure 16 shows the readout on the

spectrum analyzer obtained from the power transmission measurements performed on the DRF. A high frequency signal generator is connected to the filter at Port 1 via a 50Ω rated transmission line and connector and the output from Port 2 is connected to the spectrum analyzer using the same method. The signal generator is swept from 1GHz to 3GHz at a power output of -10dBm. The null reference of the spectrum analyzer is at approximately -57dBm before input signal is fed into the filter. The key measurement values from the analyzer are as listed in Table 4.

Fig. 16. Measured Power Transmission (1 - 3GHz).

Frequency (GHz)	Power (dBm)
1.000	-34.82
2.055	-56.48
3.000	-29.23

Table 4. Transmission Power Measurement Values.

Power delivery and attenuation is then observed at the spectrum analyzer. Comparison with the measured S(1,2), S(2,1) response showed a near accurate bandstop center frequency at 2.055GHz. Power attenuation due to lossy transmission line medium and also dielectric effects is at a combined approximate of -19.23dBm. As observed from the scattering response and measurements, there is slightly higher attenuation at the lower frequency range below 2GHz. This is the maximum insertion loss of the filter and can be calculated by using (*Eq. 2-a*). The calculations for the insertion loss of the filter at 1GHz are presented below.

$$Insertion\ Loss\ (dB) = 10\log_{10}\frac{P_R}{P_T} \tag{2-a}$$

$$Transmission\ Line\ Loss = -19.23\ dBm = \left[10^{\left(-\frac{19.23}{10}\right)}\right]\times 10^{-3} = 1.194\times 10^{-5}\ Watts$$

$$Input\ Power = -10\ dBm = \left[10^{\left(-\frac{10}{10}\right)}\right]\times 10^{-3} = 10^{-4}\ Watts$$

$$Transmitted\ Power,\ \boldsymbol{P_T} = -34.84\ dBm = \left[10^{\left(-\frac{34.84}{10}\right)}\right]\times 10^{-3} = 3.296\times 10^{-7}\ Watts$$

$$Received\ Power,\ \boldsymbol{P_R} = (Input\ Power) - (Transmission\ Line\ Loss)$$

$$= 10^{-4} - 1.194\times 10^{-5} = 8.806\times 10^{-5}\ Watts$$

$$\therefore\ Insertion\ Loss\ (dB) = 10\log_{10}\left(\frac{8.806\times 10^{-5}}{3.296\times 10^{-7}}\right) = \underline{\underline{24.27\ dB}}$$

When compared to the insertion loss that is simulated in CST which is below 10dB, the insertion loss calculated from real world power transmission measurements for the filter is higher than the simulated value. There are a few external factors that lead to the deviation of the measured results from the simulated data. The insertion loss for filters, as mentioned before is caused by lossy dielectric medium and also a non unity value of the magnitude of reflection coefficient between the two ports. The latter can also be analyzed from the Smith Chart plot for the design. The impedance curve seen in the plot in Figure 17 shows the impedance of the filter from 1GHz to 3GHz. If the filter is acting as a true short circuit for both the input and output ports at the pass band frequencies, the impedance line should be ideally running along the outer most circumference of the Smith Chart. The lost signal power is converted into heat, most of it in the dielectric medium and some from the microstrip substrate. The unwanted attenuation and insertion loss can be lowered by using high permittivity dielectric materials with lower dielectric loss on the DRF structure. However, the dielectric resonator filter works as expected with the design derived from the DRA structure. The presence of a high permittivity dielectric in the center of a radiating strip ring excites the transverse magnetic (TM) mode of resonance, thus creating a central magnetic field that induces surface current on the coupled adjacent microstrip ring.

From the Smith Chart plot obtained from the analyzer in Figure 18, the key measurement impedance values are identified respectively in Table 6 below. Comparisons from the simulated and measured impedance response of the DRF at 1-3GHz shows similar matched impedance of 50Ω at the center frequency of 2GHz. Although the overall plot pattern of the measured impedance response have less similarity towards the simulated data, both of them shows that the filter circuit is acting as a matched termination load at the notch center frequency of 2GHz. The impedance of the filter moved towards the outer radius of the Smith Chart at the other frequencies.

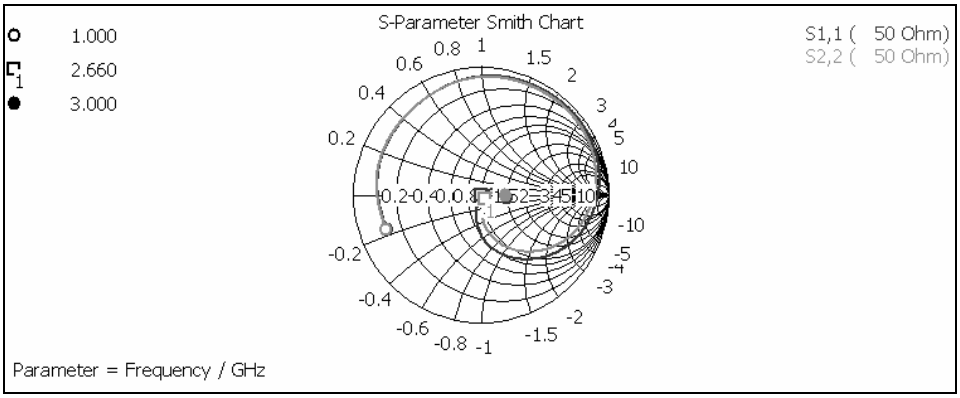

Fig. 17. Impedance Response of Structure.

Fig. 18. Measured Impedance Response of Structure.

Frequency (GHz)	Impedance (Ω)
1.000	57.166 + j 22.856
1.723	66.398 – j 2.9104
2.059	50.250 + j 0.7012
2.294	39.457 – j 7.5371
3.000	30.729 + j 9.9124

Table 6. Measured Impedance Response Values.

2.4.3 Half cylindrical pellet

In order to study the effect of the half cylindrical pellet towards the frequency response of the filter, the cylindrical pellet is replaced with a split pellet from the same batch of samples. The thickness for this pellet is sanded to the same measurements as the previous sample. Furthermore, the dielectric properties are also re-measured to make sure that it is consistent and similar to the previous pellet sample. Thus this will give a good representation of the variation of shape in a test to determine the effect of various shapes of dielectrics towards the microwave properties of the electrical model or structure. Dielectric material orientation will be similar to the previous DRA structure and the test setup for this is also shown in Figure 19.

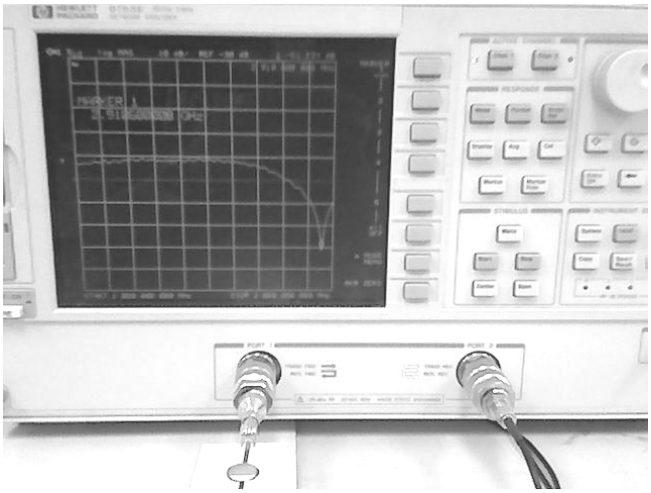

Fig. 19. DRF Measurement (Half Cylindrical Pellet).

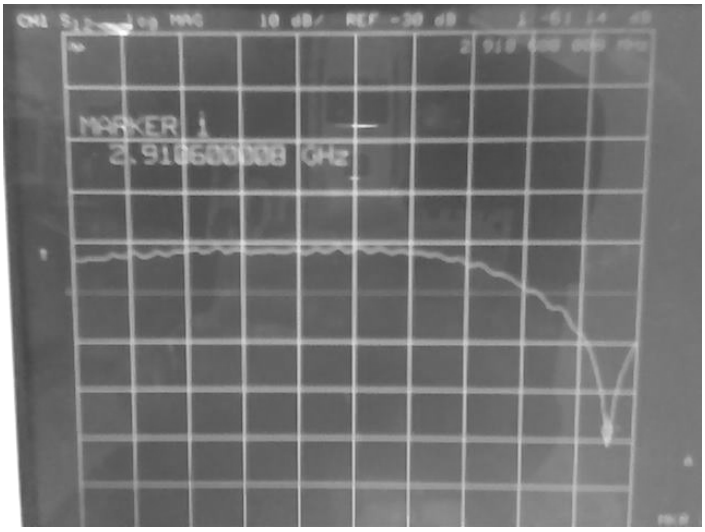

Fig. 20. Measured Frequency Response (Half Cylindrical Pellet).

The measured S(1,2) frequency response for the half cylindrical pellet is shown in Figure 20. As observed, the bandstop response curve has shifted to 2.91GHz. The return loss is measured at a lower -61.14dB compared to the previous DRF utilizing the full cylindrical dielectric pellet. From this test, it is observed that the half cylindrical dielectric material shape increases the stop frequency by almost 1GHz and lowered the stopband attenuation by 20dB. Although the network analyzer that was used for the measurements was limited to a maximum sweep frequency of 3GHz, it can be observed from the S(1,2) plot that the bandwidth of the filter remains consistent for both dielectric shapes. Thus, it can be deduced from this that splitting the dielectric material in half on the filter generally increases the notch filter center frequency by 50% and also lowers the attenuation at the center frequency also by 50%.

3. Conclusion

Results from the dielectric measurements suggest that by using 2 different synthesis techniques, different dielectric behavior of the dielectric material can be achieved. By using heat treatment, the structural properties of the material will be altered thus giving the material more radical dielectric properties. Wet chemical method on the other hand, produces normal dielectric properties on the samples with varied dopant compositions. Both methods also indicate that there is respectively, an ideal temperature and composition value for the materials to achieve their maximum dielectric properties.

The study of the trial batch of Barium Strontium Titanate samples suggests that dielectric properties of the pellet increased proportionally to the relative percentage of Strontium atoms inside the material. Measurements also indicated that the density of atoms inside the pellet affects the dielectric properties in a positive way. Another factor that greatly affects the dielectric properties of the material is the use of different degrees of heat treatment synthesis. As seen from initial tests, at 1300˚C, the atomic structural properties of dielectric material is directly affecting the dielectric permittivity of the sample. In this case, the sample has a negative real value of permittivity, also meaning that penetrating electrical fields are refracted off the material.

By using the ideal synthesis methods obtained from the study of the Barium Strontium Titanate samples, the new composition of Bismuth Lanthanum Titanate was able to be produced. Wet chemical method that was used to synthesize the BLT power was favoured over other methods as it is an easier reaction to start and volatile elements of the composition can be safely retained. The drawback of this method is that the resultant product needs to go through a calcination process in order to purify the material. This is because of the presence of organic chemicals used as solvents and chelating agents in the raw material. However this preferred method is the least complicated and can be done at typical laboratory environments without needing specialized equipment. Lanthanum ions were selected as a dopant for Bismuth Titanate because of its rare earth mineral properties. Most mineral and metals of this class exhibits very good magnetic properties such as Neodymium alloys. In conclusion, a new type of dielectric material composition has successfully been fabricated using the least complex and feasible synthesis method available. The dielectric properties of the material are also desirable and effective in microwave applications.

4. Acknowledgment

The authors would like to thank Universiti Kebangsaan Malaysia and Universiti Sains Malaysia for their technical help and support in materials procurement, DRO design and fabrication.

5. References

[1] Petosa, A., *Dielectric Resonator Antenna Handbook*, Artech House, 2007.
[2] Peixeiro, C., "Microstrip rectangular ring bandpass filter elements for GSM," *APMC2000*, 1273–1276, 2000.
[3] Wong, K.-L., *Compact and Broadband Microstrip Antennas*, John Wiley and Sons, 2002.
[4] James, J. R. and P. S. Hall, *Handbook of Microstrip Antennas*, IEE, 1989.
[5] Martin, M. A., B. S. Sharif, and C. C. Tsimenidis, "Dual frequency microstrip antenna with V slot," *Wideband and Multiband Antennas and Arrays*, IEE (Ref. No. 2005/11059), 183–184, 2005.
[6] Ping, D. E. and R. B. Dybdal, "An efficient dual frequency antenna feed," 0-7803-8302-8/04/$20.00, IEEE, 2004.
[7] Mandeep, J., N.K. Loke, S. Hassan, M. Ain, S. Sreekantan and K.Y. Cheong "Investigation of microwave properties of high permittivity ceramic substrate," *J of Electromn. Waves and Appl.*, Vol. 22, 1873–1882, 2008.
[8] Rajabi, M., M. Mohammadirad, and N. Komjani, "Simulation of ultra wideband microstrip antenna using EPML-TLM," *Progress In Electromagnetics Research B*, Vol. 2, 115–124, 2008.
[9] Mandeep, J., A. Lokesh, S. Hassan, M. N. Mahmud, and M. Ain, "Design of Cartesian feedback RF power amplifier for L-band frequency range," *Progress In Electromagnetics Research B*, Vol. 2, 207–222, 2008.
[10] Hassani, H. R. and M. Jahanbakht, "Method of moment analysis of finite phased array of aperture coupled circular microstrip patch antennas," *Progress In Electromagnetics Research B*, Vol. 4, 197– 210, 2008.
[11] Khalaj-Amirhosseini, M., "Wideband or multiband complex impedance matching using microstrip nonuniform transmission lines," *Progress In Electromagnetics Research*, PIER 66, 15–25, 2006.
[12] Wang, S., X. Guan, D.Wang, X. Ma, and Y. Su, "Electromagnetic scattering by mixed conducting/dielectric objects using higherorder MOM," *Progress In Electromagnetics Research*, PIER 66, 51–63, 2006.
[13] Liao, S. L. and R. J. Vernon, "On the image approximation for electromagnetic wave propagation and PEC scattering in cylindrical harmonics," *Progress In Electromagnetics Research*, PIER 66, 65–88, 2006.
[14] Moeckly, B. H. and Y. Zhang, "Strontium Titanate thin films for tunable YBCO microwave filters," IEEE Trans. Appl. Supercond., Vol. 11, 450-453, 2001.
[15] Boutayeb, H., A.-C. Tarot, and K. Mahdjoubi, "Focusing characteristics of a metallic cylindrical electromagnetic band gap structure with defects," *Progress In Electromagnetics Research*, PIER 66, 89–103, 2006.
[16] Khalaj-Amirhosseini, M., "Microwave filters using waveguides filled by multi-layer dielectric," *Progress In Electromagnetics Research*, PIER 66, 105–110, 2006.

[17] Rezaei, P., M. Hakkak, and K. Forooraghi, "Design of wideband dielectric resonator antenna with a two-segment structure," *Progress In Electromagnetics Research*, PIER 66, 111–124, 2006.

[18] Chen, H., L.-X. Ran, B.-I. Wu, J. A. Kong, and T. M. Grzegorczyk, "Crankled S-ring resonator with small electrical size," *Progress In Electromagnetics Research*, PIER 66, 179–190, 2006.

[19] Sihvola, A. H., "Peculiarities in the dielectric response of negative permittivity scatterers," *Progress In Electromagnetics Research*, PIER 66, 191–198, 2006.

Microstrip Antennas

Edited by Prof. Nasimuddin Nasimuddin

ISBN 978-953-307-247-0
Hard cover, 540 pages
Publisher InTech
Published online 04, April, 2011
Published in print edition April, 2011

In the last 40 years, the microstrip antenna has been developed for many communication systems such as radars, sensors, wireless, satellite, broadcasting, ultra-wideband, radio frequency identifications (RFIDs), reader devices etc. The progress in modern wireless communication systems has dramatically increased the demand for microstrip antennas. In this book some recent advances in microstrip antennas are presented.

INTECH
open science | open minds

InTech Europe
University Campus STeP Ri
Slavka Krautzeka 83/A
51000 Rijeka, Croatia
Phone: +385 (51) 770 447
Fax: +385 (51) 686 166
www.intechopen.com

InTech China
Unit 405, Office Block, Hotel Equatorial Shanghai
No.65, Yan An Road (West), Shanghai, 200040, China
中国上海市延安西路65号上海国际贵都大饭店办公楼405单元
Phone: +86-21-62489820
Fax: +86-21-62489821